J. Earth Syst. Sci. (2020)129 30
https://doi.org/10.1007/s12040-019-1277-4

© Indian Academy of Sciences

Susceptibility assessment of rainfall induced debris flow zones in Ladakh–Nubra region, Indian Himalaya

H S Negi*, Anant Kumar, N Narasimha Rao, N K Thakur, M S Shekhar and Snehmani

Snow and Avalanche Study Establishment, Him-Parisar, Sector-37A, Chandigarh 16036, India.
**Corresponding author. e-mail: hs.negi@sase.drdo.in*

MS received 17 April 2019; revised 29 July 2019; accepted 4 August 2019

In recent past, rainfall-induced debris flow events in Ladakh–Nubra region have caused loss of lives and damages to civil infrastructures and army locations. Therefore, there is a need of high spatial and temporal monitoring of precipitation, and further to assess susceptible rainfall-induced debris flow zones in the area. We assessed the rainfall data collected at two gauge stations and observed a significant increase in the rainfall amount over the study region during summer-monsoonal period 1997–2017. Increasing trend was also observed from CRU gridded precipitation dataset. A GIS-based multi-criteria evaluation (MCE) method was performed by combining topographical, environmental and hydrological parameters for mapping of rainfall-induced susceptible zones. Suitability analysis of precipitation forecasts from WRF model at higher resolution (3 km) was also performed. A good agreement (r = 0.76) was observed between 4-day model forecast and field observed rainfall. Further, the simulated precipitation from WRF was incorporated into GIS model for assessment of debris flow susceptible zones for two cases of heavy precipitation events. The modelled high, medium, low and very low risk susceptible zones identified for the year 2015 events are validated with field survey and pre-post satellite imageries, and found in good agreement (ROC = 76.6%). The model was able to identify affected areas during the Leh cloud burst event in year 2010. In addition, a threshold value of rainfall for initiation of debris flow in the region was also reported.

Keywords. Debris flow; Karakoram–Himalaya; rainfall; WRF; CRU; weighted overlay.

1. Introduction

Debris flow and landslide triggered due to heavy or prolonged rainfall are amongst the most devastating hazards over the Himalayan region as these are responsible for economic loss, injuries and loss of lives during the monsoon season (Bookhagen and Burbank 2010; Bhan *et al.* 2015). In recent past during first week of August 2010, Leh district experienced 2 hrs of concentrated rainfall reaching a peak intensity of ∼75 mm over a 30-min period (Hobley *et al.* 2012), which triggered various mass movement events in the region and caused large scale destruction and several deaths (Juyal 2010). Similarly, during 15–17 June 2013, torrential rainfall triggered numerous landslides and debris flows in and around Uttarkashi districts, claimed lives of more than 5700 people (Martha *et al.* 2015). In another event, heavy rainfall triggered debris flows at numerous places of Darjeeling Himalaya in June–July month of 2015 and claimed lives of 38 people (Biswas and Pal 2016). More recently in July 2019, landslide events triggered by incessant

Published online: 20 December 2019

monsoonal rains across Nepal have claimed 78 lives and displaced 17,500 others in the year 2019 ('Nepal floods': Pradhan 2019). Above-mentioned studies and reports suggest dominant role played by rainfall in triggering debris flow and landslide events. In addition, a few such activities may also get induced by tectonic activities (Adhikari and Koshimizu 2005) and lake/stream burst (Owen *et al.* 2008). Under on-going climate change, any possible shift in the rainfall pattern over the Himalayas may lead to upsurge in frequency and intensity of these hazardous events (Bhutiyani *et al.* 2010). Thus, it becomes imperative to understand the threat posed by heavy or prolonged rainfall, especially for the region under low rainfall zone, where level of preparedness may not be high by weather forecasters or disaster management authorities (Ziegler *et al.* 2016). One such area situated in Nubra–Ladakh region, which is currently facing increased vulnerability to climate hazards and related risks (Barrett and Bosak 2018). After deadlier 2010 event in Leh, another heavy rainfall event occurred during first week of August 2015 in Nubra region, where continuous rainfall caused series of debris movement at various places of the valley. Both of these events have damaged various civil infrastructures and army locations in the region. Despite threatening debris flow events in the region, the susceptibility maps are not available for most of the area, which can be used for hazard assessment and mitigation.

Different studies suggest that debris flows susceptibility depends on several causative factors, which include environmental, hydrology, topography, geology, etc. (Ventra and Clarke 2018; Crosta and Frattini 2003). The causative factors are usually selected based on the analysis of debris flow types and the characteristics of the study area (Wang *et al.* 2019). These factors may be further categorized into various levels (primary, secondary, etc.) as per their potentiality in triggering debris flow events (Dou *et al.* 2015). Prime triggering factor, i.e., rainfall facilitates the downward movement of the solids (boulders, rocks, etc.) or soils on steep slopes by increasing pore water pressure, seepage force and reducing effective stress of the soils (Lu *et al.* 2012). Consequently, real-time tracking of rainfall observations is critical for assessment and early monitoring of rainfall-induced hazards (Huffman *et al.* 2007; Gebremichael and Hossain 2010). Yet, many parts in high-risk area of Himalayas lack resources to maintain the extensive weather networks required to successfully observe these conditions. In recent years, space-borne platforms and computing technologies are effectively employed for hazard detection, monitoring and susceptibility assessment over complex terrain (Pardeshi *et al.* 2013). Remotely sensed gridded precipitation datasets such as Global Precipitation Measurements (GPM) and Tropical Rainfall Measuring Mission (TRMM) offer high temporal and spatial scales to improve the understanding of landsliding and debris flow events (Nikolopoulos *et al.* 2014; Kirschbaum and Stanley 2018). Apart from rainfall measurements, optical remote sensing imageries such as Landsat, Advanced Space-borne Thermal Emission and Reflection Radiometer (ASTER), Sentinel-2, etc., and digital elevation models (DEMs) such as Shuttle Radar Topographic Mission (SRTM), ASTER GDEM, etc., are widely adopted to retrieve aforementioned factors like land use/land cover (LU/LC), drainage, slope, curvature, vegetation, etc. (Elkadiri *et al.* 2014).

Blais-Stevens and Behnia (2016) suggested the quantitative and qualitative techniques to develop debris flow susceptibility map. Quantitative techniques such as logistic regression model (Chauhan *et al.* 2010), frequency-ratio model (Khan *et al.* 2019), fuzzy logic (Kayastha *et al.* 2013), etc., depend on probability of sliding by studying the relationship between causative factors and past debris flow events. Qualitative techniques such as analytical hierarchical process (AHP) and weighted overlay analysis (WOA) are mostly employed for regional scale assessment (Kayastha *et al.* 2013). These techniques consider ranking and weighting of various causative factors based on expert opinion about an area (Saaty 1990). Qualitative techniques have been extensively studied for hazard susceptibility mapping over the Himalayan region (Basharat *et al.* 2016; Shit *et al.* 2016; Kanwal *et al.* 2017). However, most of these studies have utilized static predictors to generate hazard susceptibility maps. In order to reduce the impact of rainfall-induced hazards, there is a need to develop linking the above qualitative GIS model output with operational weather forecasts (Liao *et al.* 2010). To quantify the spatial and temporal variability in rainfall at regional scales, Numerical Weather Prediction (NWP) models have the added advantage of weather forecasting and thus can help in debris flow and landslide hazard predictions (Ochoa *et al.* 2014). Weather Research and Forecasting (WRF), a numerical mesoscale model

(Mourre *et al.* 2016) has the potential to simulate heavy rainfall events. Over Himalayan region, Kumar *et al.* (2012) simulated 2010 'Leh cloud burst event' using WRF model and observed that changing the microphysics schemes inside the model could result into better simulation. Later on, Thayyen *et al.* (2013) studied this cloud burst event using atmospheric modelling and hydrological analysis to re-establish rainfall estimates during the event.

The present study thus focuses on susceptibility assessment of debris flow zones in Ladakh–Nubra region. We studied summer precipitation pattern over this region using ground observatories as well as gridded precipitation data from Climate Research Unit (CRU) for a common period 1997–2017. GIS based multi-criteria evaluation (MCE) technique has been performed based on static as well as dynamic predict or to identify debris flow susceptible zones. WRF forecasts have been incorporated into GIS model for two cases of heavy precipitation events. Modeled high, medium, low and very low risk susceptible zones were evaluated and validated during field visit and satellite imageries.

2. Study area

The study focuses on Ladakh–Nubra region of Indian part of Karakoram Himalaya (KH), having the geographical extension between latitude 34.00°–35.25°N and longitude 76.75°–78.00°E (figure 1) and covers an area of ∼4895 km^2. The valley originates from south-western part of Tibetan Plateau and runs over major thrust zone formed between Karakoram and Zanskar ranges, thus stretching through Kargil, Zanskar, Leh and Nubra. Physiography of the terrain is harnessed with snow-covered peaks, glaciers and non-glaciated valleys. Lying on the rain shadow area of Himalayas, the Nubra region combines the condition of both arctic and desert climate (Chundawat and Rawat 1994; Negi 1995). There is a wide diurnal and seasonal fluctuation in temperature with −40°C in winter to +35°C in summer with relative humidity ranging between 6% and 24% (Raj 2013). Precipitation occurs mainly under the influence of westerly disturbances in winter and due to induced south-west monsoon during summer in lower reaches of valley (Bhutiyani *et al.* 2010). Being in the rain shadow region, devoid of vegetation and full of sediments due to glaciated valley, during the abnormal monsoon years, the southwest summer monsoon penetrate into this region and mobilize large scale sediments in the form of debris flow from unprotected mountain slopes (Juyal 2010). The variation in slope alongside road (between 22° and 50°), make this region highly sensitive and vulnerable to various mass movements.

2.1 *Leh–Nubra valley road connectivity*

The main road access to Nubra Valley is through Khardung-La pass (figure 1b) which is also amongst one of the highest motorable roads in the world. The road connectivity has a huge impact for locals residing in the Nubra valley and has helped in bringing changes in socio-economic condition. The road to Nubra via Khardung-La does not provide all weather connectivity as it gets closed during heavy snowfall in winter months and thus the region is completely cut off for some period. Also various rainfall-induced debris movement, landslides and rock falls during summer causes frequent road blockage.

3. Data used

3.1 *Precipitation dataset*

3.1.1 *In-situ rain gauge observations*

Snow and Avalanche Study Establishment (SASE), India has a snow-meteorological observatory in this region at Sasoma. Rainfall data is being measured using accumulation rain gauge at this observatory since year 2000. The rainfall data collected on daily scale was analysed for the summer months (June–September). In addition, rainfall information available from Indian Air Force (IAF) station at Thoise was also utilised.

3.1.2 *Gridded precipitation from CRU*

The most recent version of the CRU-TS ver. 4.02 precipitation data available from University of East-Anglia has been utilized in this study (https://crudata.uea.ac.uk/cru/data/hrg/). The data is entirely based on gauge information and consist of monthly gridded fields of precipitation at 0.5° grid spacing over land areas. The CRU dataset is popular because of its relatively long history and fine spatial resolution of 0.5°. These datasets are continuously updated through support from World

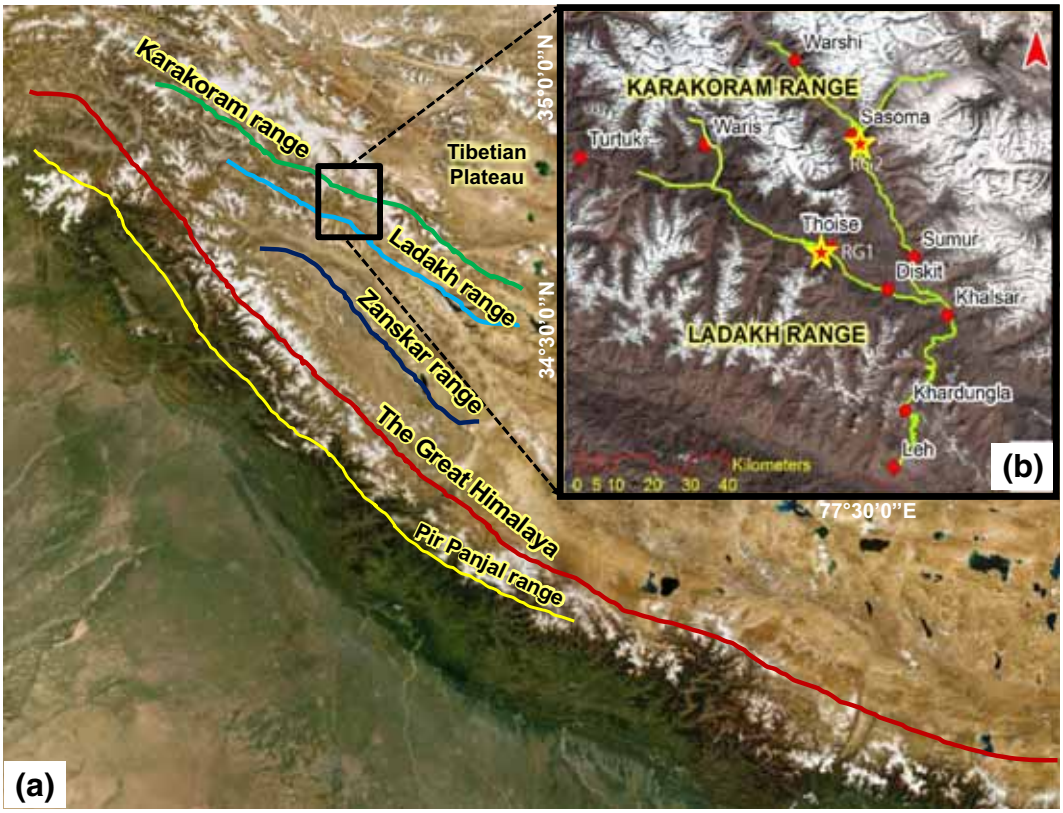

Figure 1. (**a**) Location of the study area on Google Earth Imagery. (**b**) Ladakh–Nubra region shown on Landsat 8 imagery with road connectivity from Leh to Nubra via Khardungla. Important places of this region are shown by red circles and star shows rain gauge stations RG1 (Thoise) and RG2 (Sasoma).

Meteorological Organization (WMO) in collaboration with the US National Oceanographic and Atmospheric Administration (NOAA) (Harris *et al.* 2014). The suitability of this dataset over North-West Himalaya has recently been carried out by Negi and Kanda (2019). Thus, the dataset was extracted for Nubra region to study summer precipitation climate variability.

3.1.3 *WRF simulation*

The high resolution non-hydrostatic Advanced Research WRF (ARW; Skamarock *et al.* 2008) mesoscale model (version 3.9) developed at National Centre for Atmospheric Research (NCAR) is used to simulate the heavy rainfall cases. In the present study, double two-way nested domains with horizontal resolution 09 and 03 km, keeping study area and its adjoining areas as the center has been used. The configuration used to run the model is depicted in table 1. The initial and lateral boundary conditions were obtained from final reanalysis data (FNL) at 1° × 1° of National Center for Environmental Prediction (NCEP) Global Forecast System (GFS; https://doi.org/10.5065/D6M043C6).

Table 1. *WRF model configurations used in the study.*

Options	WRF v3.9
Horizontal resolution	9 and 3 km
Microphysics	WSM6
Long wave radiation	RRTM
Shortwave radiation	Dhudhia
PBL physics	YSU
Land surface model	Noah land-surface model
Cumulus parameterizations	Kain–Fritsch
Vertical levels	40
Model static fields	USGS
IC and BC	NCEP GFS (0.25° × 0.25°)

3.2 *Causes and associated factors*

Different causative factors for debris flow movement can be divided into three groups consisting topographical, environmental and hydrological (figure 2). The final susceptibility map involves the generation of thematic maps of various causative factors.

3.2.1 *Topographical*

Topographical factors include slope, aspect and curvature derived using Advanced Space-borne

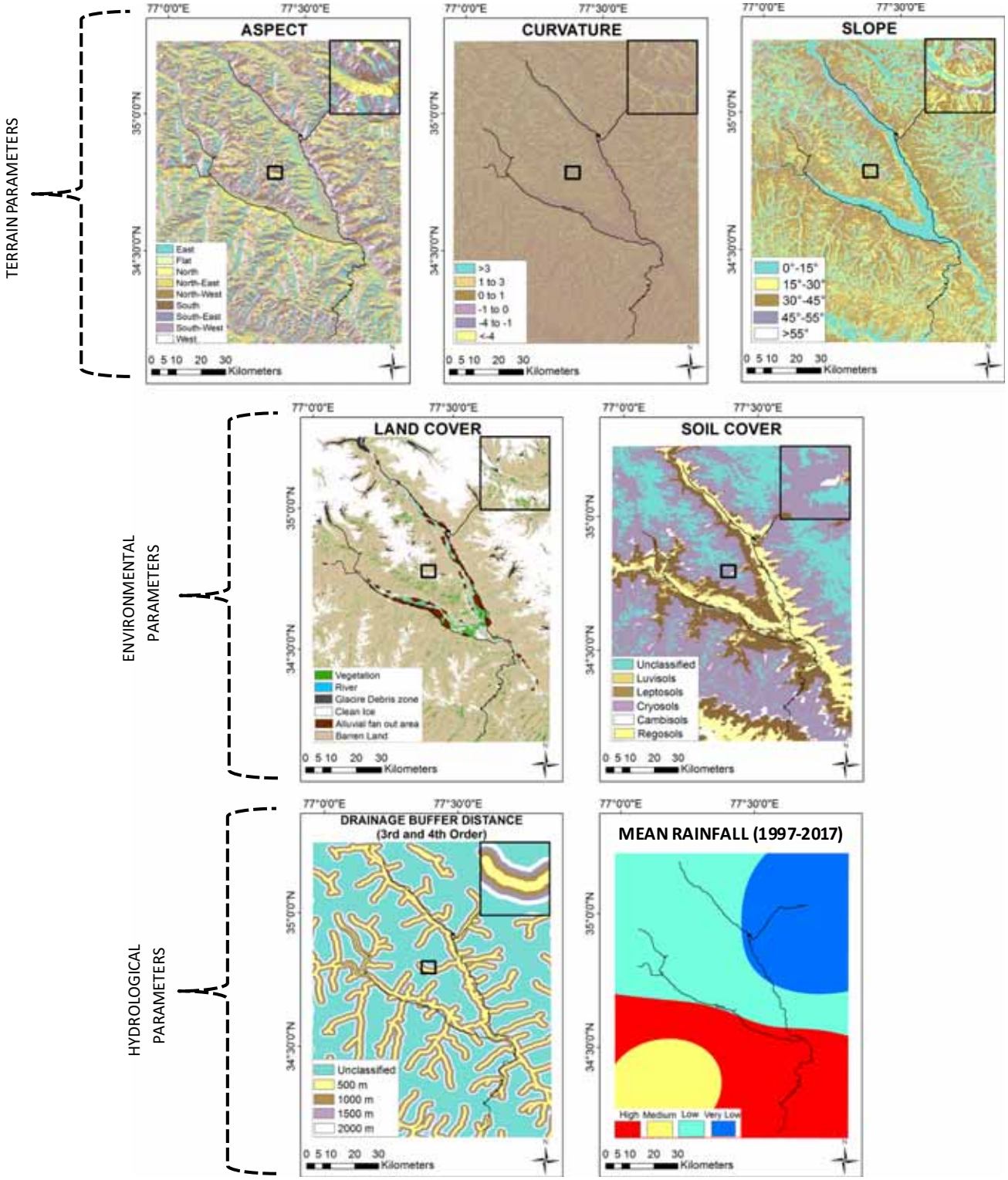

Figure 2. Thematic layers of terrain, environmental and hydrological parameters considered for mapping debris flow zones. Square black box in the figures represents the zoomed portion.

Thermal Emission and Reflection Radiometer (ASTER) digital elevation model (DEM). One of the important factor, i.e., slope gradient was derived in degrees ranging from 0° to >55°. Aspect determines the direction of terrain slope w.r.t. north. Nine classes of aspect were prepared depending on the direction of slope. Over lower reaches of Nubra valley, induced monsoon rainfall has more impact on south directing hill slopes compared to other directions which makes hill

slopes facing south-east or south-west more prone to debris flows (Riaz *et al.* 2018). Curvature of slope is responsible for controlling the flow of water during rainfall. It is one of the prime contributing factors for slope failure during shallow landsliding event. During analysis, curvature was classified as concavity and convexity based on planar profiles. Concave slopes with high negative values tend to retain water for a longer period of time after rainfall and this causes loosening of top layer soil (Vijith *et al.* 2013).

3.2.2 *Environmental*

Land cover and soil classes were considered under environmental factors. Landsat-8 surface reflectance imagery acquired on 30th August, 2015 with cloud coverage less than 10% was downloaded from USGS Earth explorer (https://earthexplorer.usgs.gov). The freely available Landsat-8 surface reflectance (SR) products are atmospherically and radiometrically corrected using Landsat Surface Reflectance Code (LaSRC) (Dwyer *et al.* 2018). Employing unsupervised classification technique, major land cover zones were mapped in Ladakh–Nubra region and following categories were generated: barren land, alluvial fan out area, clean ice, glacier debris zone, vegetation and river. Debris flow is an outcome of large quantities of ice-cored glacial sediments which gets easily activated from heavy precipitation, snowmelt and glacial lake outbursts (Haeberli *et al.* 1997). Since it originates mainly from the lower ablation region of glaciers, debris zone of glaciers was considered as separate land cover class. In addition, alluvial fan areas, which are triangle-shaped deposit of gravel, sand/silt, and sediment are usually created by flowing water interaction with mountains, are considered as another class. Road connectivity to different places mainly passes through these fans out areas which frequently get affected during summer rainfall period (figure 3). Other classes such as barren land, vegetation and water bodies are well defined land cover classes (Congalton *et al.* 2014). Slope variation over barren land was found varying between 36° and 55°, which makes it susceptible to various landsliding events as it cannot hold the soil firmly. Vegetation areas are considered under less susceptible class as it reduces the impact of landslide events by providing necessary stability through their roots.

Soil cover information was taken from global soil information system called “Soil Grids” released by International Soil Reference Information Centre (ISRIC) (https://www.isric.org/explore/soilgrids). The Soil Grids at 250 m spatial resolution are outputs of a system for automated global soil mapping based on state-of-the-art spatial prediction methods (Hengl *et al.* 2017). It provides global predictions for standard soil properties such as organic carbon, bulk density, cation exchange capacity (CEC), pH, soil texture fractions and coarse fragments at seven standard depths along with predictions of depth to bedrock and distribution of soil classes based on World Reference Base (WRB) and United States Department of Agriculture (USDA) classification systems. For the study region, soil type consists of five main classes: Luvisols, Leptosols, Regosols, Cambisols, and Cryosols. Properties of these soil classes were collected from various literatures and have been discussed in table 2, which were also validated during field survey in the study region. From figure 3, we can see the soil class Leptosols and Regosols along road connectivity to Sasoma. Compared to these two classes, other classes such as Luvisols, Cryosols and Cambisols are less susceptible to debris movement.

3.2.3 *Hydrological*

Intensive as well as short duration continuous rain has caused various debris flow events in Ladakh region during recent past. Therefore, long-term and short-term period thematic summer precipitation information was produced from CRU and WRF model respectively.

Stream networks are considered another important factor during debris flow events as they contribute towards erosion of the slope and also saturate the underwater section of the materials (Miller and Burnett 2008). The stream network of the study area was computed using ASTER DEM. Four buffer zones with 500 m intervals were produced from the stream networks to see the impact of distance. It was observed that the stream order third and fourth contributes maximum to erosion on roadside slopes ranging 30°–45°.

3.3 *Field survey and validation*

Field survey was carried out in the study region during September 2015 (post-debris flow events) and locations were captured using Trimble Juno GPS. Further, Optical Land Imager (OLI) sensor

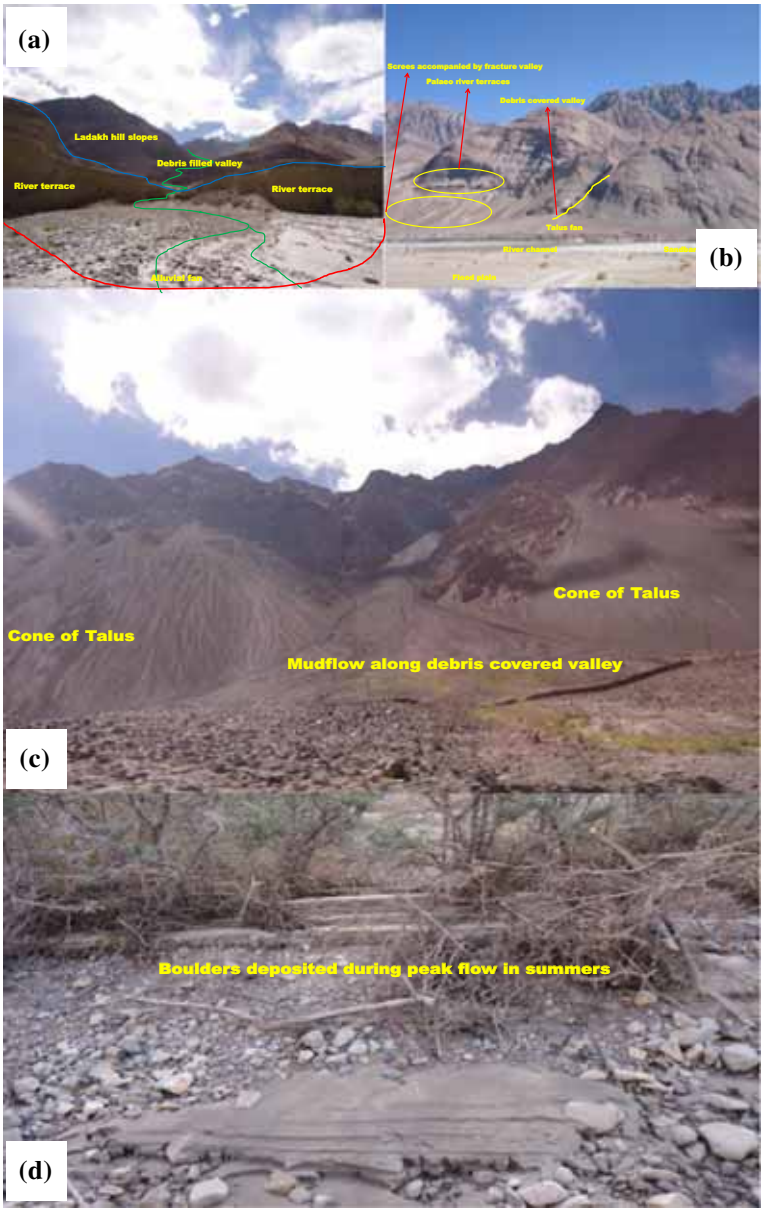

Figure 3. (**a**) Debris field valley comprising mostly rock pieces mixed with clayey and sandy soil. (**b**) Older, well compacted, naturally formed alluvial filled fan out area (Talus fan). (**c**) Mud flow in the lower part of the debris covered valley. (**d**) Boulders deposition during period of peak discharge.

data from Landsat 8 was also utilized to observe pre- and post-debris flow changes.

4. Methods

4.1 *Precipitation analysis*

To assess the influence of summer precipitation on debris flows, it is important to study climatic pattern over the region. Field observational study on precipitation for Nubra region is rather limited (Chevuturi *et al.* 2015). Therefore in the present study, the summer precipitation information available from two stations was analysed. Further, gridded precipitation data from CRU was also studied for the summer periods. The NetCDF data format of CRU was converted into Geo-TIFF format before analysis. The trend for cumulative summer precipitation from CRU data in the study region was analysed for the similar period 1997–2017.

The early-warning for debris flow events can be generated based on the temporal aspects of slope failures (Liao *et al.* 2010). Thus, an effort has been made in the present study to assess the suitability of

Table 2. *ISRIC soil classes for Nubra region along with their properties.*

Soil class	Properties
Luvisols	Porous and well aerated topsoil
	High available water content
	Water stagnation increases over the time period
	When on slopes, prone to top soil erosion
Leptosols	Are extremely gravelly (>80% gravel, stones, boulders by volume)
	Low water holding capacity due to limited depth and extreme coarse structure
	On steep slopes, prone to erosion
Regosols	Undeveloped, medium textured soil
	Consists of alluvial materials
	Structureless due to lack of cohesion between soil particles
	Often prone to erosion
Cambisols	Good structural stability
	Not much prone to erosion
	Good internal drainage
Cryosols	Occurrence of variable amount of ice in the sub soil
	Thawing phenomenon lead to irregular land surface
	Soils with evidence of freezing or thawing

WRF simulations for rainfall triggered debris flow during heavy rainfall events. The following two cases were taken to simulate heavy rainfall events:

(a) In 2015, this region experienced destructive storm and continuous rainfall in first week of August and was subsequently hit by series of debris flows and flash floods. Amount of the daily rainfall intensity was simulated from WRF and compared with field data. WRF forecasted 5-day cumulative precipitation layer was generated for aforementioned heavy rainfall event and later incorporated into GIS model.

(b) In 2010, intense rainfall occurred in various places of Ladakh during the period 1–5th August which triggered deadly flash floods and debris flows. Destruction was concentrated in areas located proximal to the mountain slopes and dried channels (Juyal 2010). The event caused at least 234 deaths in the Ladakh region (Ziegler *et al.* 2016). Another 800 were reported missing post-landsliding event as per army hospital records (Gupta *et al.* 2012).

The sensitivity of various WRF configurations in simulating heavy rainfall events is assessed using the Noah land surface model (LSM) (table 1) (Tewari *et al.* 2004). The ability of WRF model configuration to simulate heavy rainfall event was evaluated by comparing the simulated rainfall with the observations through indicators such as mean absolute error (MAE) and root mean square error (RMSE).

4.2 *Mapping of debris flow susceptible zones*

For mapping susceptible zones, multi-criteria evaluation (MCE) method was used. Weighted overlay analysis (WOA) was implemented in ArcGIS environment as it is a simple and reliable technique (Riad *et al.* 2011). This technique involves overlaying of several raster files (causative factors) to produce single output by assigning weight of each raster according to their importance (Saaty 1980). Overall sum of the weight of causative factors must be equal to 100 after comparison. The thematic layers of various topographical, environmental and hydrological factors were reclassified and rating value between 1 and 9 (1 being least susceptible and 9 most susceptible to landslides) was assigned to each class based on their potential to trigger debris flows (Calligaris *et al.* 2013). Pair-wise comparison matrix was created to find weight values and their results are shown in figure 4. Weights were calculated for each causative factors after inter- and intra-comparison (table 3). Assigning the weights and rank values for each classes were based on expert opinions, field observations and previous published literatures (Lepore *et al.* 2011; Calligaris *et al.* 2013; Long and De Smedt 2019).

(a)

RAINFALL	High (>200 mm)	Medium (100-200 mm)	Low (50-100 mm)	Very Low (<50 mm)
High (>200 mm)	1.00	3.00	5.00	7.00
Medium (100-200 mm)	0.33	1.00	3.00	5.00
Low (50-100 mm)	0.20	0.33	1.00	3.00
Very Low (<50 mm)	0.14	0.20	0.33	1.00

SLOPE	30-45	15-30	45-55	>55	0-15
30-45	1.00	4.00	6.00	7.00	9.00
15-30	0.25	1.00	3.00	5.00	7.00
45-55	0.17	0.33	1.00	4.00	5.00
>55	0.14	0.20	0.25	1.00	3.00
0-15	0.11	0.14	0.20	0.33	1.00

SOIL CLASS	Regosols	Leptosols	Luvisols	Cambisols	Cryosols
Regosols	1.00	3.00	4.00	6.00	8.00
Leptosols	0.33	1.00	3.00	5.00	7.00
Luvisols	0.25	0.33	1.00	5.00	7.00
Cambisols	0.17	0.20	0.20	1.00	4.00
Cryosols	0.17	0.14	0.14	0.25	1.00

LAND COVER	Alluvial fan out area	Glacier Debris Zone	Barren Land	Clean Ice	Vegetation	River
Alluvial fan out area	1.00	3.00	5.00	7.00	8.00	9.00
Glacier Debris Zone	0.33	1.00	3.00	5.00	6.00	9.00
Barren Land	0.20	0.33	1.00	5.00	5.00	7.00
Clean Ice	0.14	0.20	0.20	1.00	5.00	7.00
Vegetatation	0.13	0.17	0.20	0.20	1.00	5.00
River	0.11	0.11	0.14	0.14	0.20	1.00

DRAINAGE BUFFER	500	1000	1500	2000
500	1.00	3.00	5.00	7.00
1000	0.33	1.00	3.00	5.00
1500	0.20	0.33	1.00	3.00
2000	0.14	0.20	0.33	1.00

CURVATURE	<-4	-4 to -1	>3	1 to 3	-1 to 0	0 to 1
<-4	1.00	3.00	5.00	7.00	8.00	9.00
-4 to -1	0.33	1.00	3.00	4.00	5.00	7.00
>3	0.20	0.33	1.00	4.00	4.00	6.00
1 to 3	0.14	0.25	0.25	1.00	3.00	5.00
-1 to 0	0.13	0.20	0.25	0.33	1.00	3.00
0 to 1	0.11	0.14	0.17	0.20	0.33	1.00

ASPECT	South-West	West	South	North-West	South-East	East	North	North-East	Flat
South-West	1.00	2.00	3.00	4.00	5.00	6.00	7.00	8.00	9.00
West	0.50	1.00	3.00	4.00	5.00	6.00	7.00	8.00	9.00
South	0.33	0.33	1.00	3.00	4.00	5.00	6.00	7.00	8.00
North-West	0.25	0.25	0.33	1.00	2.00	4.00	5.00	6.00	8.00
South-East	0.20	0.20	0.25	0.50	1.00	4.00	5.00	6.00	8.00
East	0.17	0.17	0.20	0.25	0.25	1.00	3.00	5.00	7.00
North	0.14	0.14	0.17	0.20	0.20	0.33	1.00	4.00	7.00
North-East	0.13	0.13	0.14	0.17	0.17	0.20	0.25	1.00	7.00
Flat	0.11	0.11	0.13	0.13	0.13	0.14	0.14	0.14	1.00

(b)

	Rainfall	Land cover	Soil	Slope	Drainage	Curvature	Aspect
Rainfall	1.00	3.00	3.00	4.00	5.00	7.00	7.00
Land cover	0.33	1.00	3.00	4.00	7.00	8.00	8.00
Soil	0.33	0.33	1.00	3.00	6.00	7.00	8.00
Slope	0.25	0.25	0.33	1.00	3.00	5.00	6.00
Drainage	0.20	0.14	0.17	0.33	1.00	4.00	2.00
Curvature	0.14	0.13	0.14	0.20	0.25	1.00	2.00
Aspect	0.14	0.13	0.13	0.17	0.50	0.50	1.00

Figure 4. Pair-wise comparison matrix for (**a**) each causative factors and (**b**) thematic layers.

Table 3. *Weights of main criteria and degree of preference for reclassified sub-criteria.*

	Main criteria		Subcriteria		
Group	Criteria (S_{ij})	Weight (W_i)	Reclassification	Weight (%)	Importance
Topographical	Slope	20%	0–15	3.3	1
			15–30	23.4	6
			30–45	52.6	9
			45–55	14.3	4
			>55	6.4	2
	Aspect	2%	Flat	1.0	1
			North	4.3	2
			North-east	4.0	2
			East	6.1	3
			South-east	9.7	5
			South	16.2	7
			South-west	22.3	9
			West	20.4	8
			North-west	16.0	6
	Curvature	5%	<−4	45.2	9
			−4 to −1	32.2	7
			−1 to 0	2.1	3
			0 to 1	1.3	2
			1 to 3	7.5	4
			>3	11.7	5
Environmental	Land cover	15%	Vegetation	3.6	2
			River	1.3	1
			Glacier debris	27.4	8
			Clean ice	12.4	4
			Alluvial fan	33.0	9
			Barren land	22.3	7
	ISRIC soil classification	23%	Luvisols	17.4	6
			Leptosols	32.0	8
			Regosols	40.3	9
			Cambisols	6.8	4
			Cryosols	3.5	1
Hydrological	Rainfall	28%	High	55.8	9
			Medium	26.3	6
			Low	12.2	3
			Very low	5.7	1
	Drainage buffer	7%	Unclassified	1.2	1
			500 m	43.5	9
			1000 m	30.1	7
			1500 m	19.6	5
			2000 m	5.6	2

Having determined the average summer precipitation for the region during 1997–2017, the amount was further divided into four ranges. The area receiving highest amount of summer precipitation (>175 mm) was likely to be more susceptible towards debris flow hazard. Earlier Chevuturi *et al.* (2015) also reported that Leh has the maximum precipitation during the monsoon period (JAS) which also comprises extreme precipitating events. Thus, rainfall was observed as the heaviest weighted factor (28%). It was then followed by the soil class (23%) and slope (20%) since after heavy precipitation event mostly rock pieces mixed with clayey and sandy soils were observed over fan out area. Maximum coverage was observed by the soil class Regosols (medium textured, eroded soil consisting alluvial materials) and Leptosols (>80% gravels, stones, and boulders by volume). Both these soil classes often get eroded during summer either due to snow/glacier melting or period of

heavy rainfall. Slope gradient influences soil water content, formation and potential for the erosion. Generally, slopes with high gradient are expected to have more influence on debris movements. On the gentle slopes where shear stress is also low, debris movements are not expected (Basharat *et al.* 2016). Curvature and aspect were seen amongst the least weighted factor. Once the above computation was achieved, final landslide susceptibility index map was produced using the following equation (equation 1).

$$\mathrm{WOA} = \frac{\sum W_i S_{ij}}{\sum W_i} \quad (1)$$

where W_i is the raster weight of importance given to each factor, S_{ij} is the reclassified raster in common criteria scale and WOA represents landslide susceptibility index map.

4.3 *Precipitation threshold estimation for debris flow event*

Precipitation thresholds for a region may indicate the value which when reached is likely to trigger debris flow events. These thresholds can be established using historical data on landslide causing rainfall events and corresponding landslide records. The precipitation threshold value can be estimated using following categorized parameters:

(i) intensity and duration (I–D)
(ii) total rainfall
(iii) rainfall event-duration and
(iv) rainfall event-intensity (Mathew *et al.* 2014).

Our approach to estimate threshold value during heavy rainfall event was based on 5-day total rainfall information estimated using WRF and ground station. Cumulative rainfall (mm/day) was calculated till event occurrence day from WRF and station data.

5. Results and discussion

5.1 *Climatological analysis of rainfall*

The climatological analysis of observed summer rainfall data showed rise in monsoonal rainfall during study period (figure 5a). The average annual rainfall is found to be 28 and 19 mm/season at Sasoma and Thoise station respectively. For both the stations increasing rainfall amount is observed with slope values +2.10 mm/season at Sasoma and +0.45 mm/season at Thoise. Sudden increase in

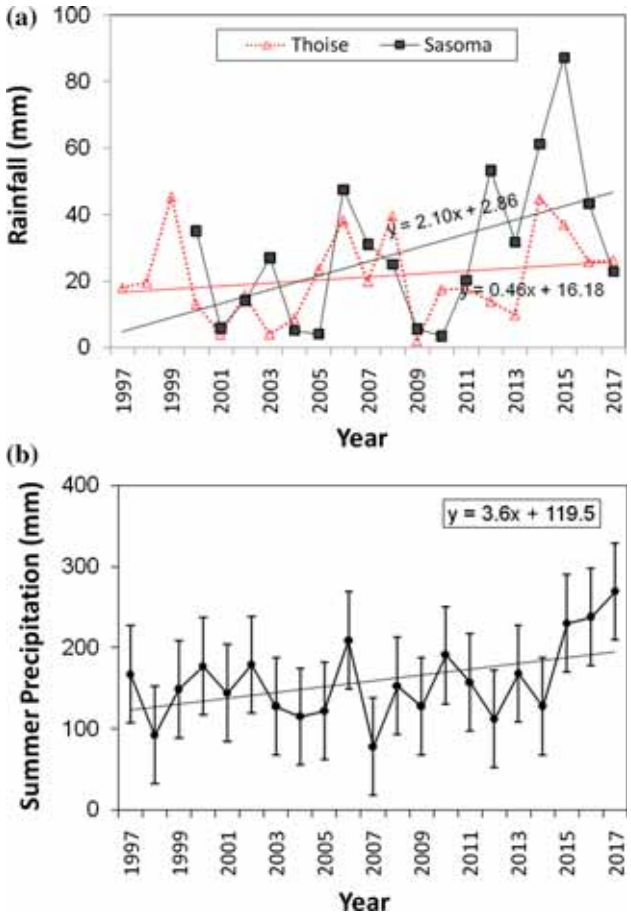

Figure 5. Rainfall trend during summer-monsoon period (JJAS) from 1997 onwards. (**a**) Rainfall data collected at Thoise (RG1) and Sasoma (RG2); and (**b**) CRU gridded data averaged for Ladakh–Nubra region.

rainfall amount is observed at both stations post year 2010. The maximum rainfall amount is found during the years 2014 and 2015, which reached up to 90 mm/season at Sasoma and 45 mm/season at Thoise. These identified heavy precipitation years may be considered exceptional as there is a general opinion that monsoon flow does not reach to upper part of Ladakh region (Bhan *et al.* 2015). Rising trend (+3.6 mm/season) in summer precipitation is also observed from CRU dataset for the same period with some bias with respect to field observation (figure 5b). Again, the maximum summer precipitation is observed for the year 2015 which led number of rainfall-induced debris flow events in this year.

The weather activity of Ladakh is affected mainly by western disturbances and less by monsoonal rainfall. As upper part of Ladakh comes under a very low rainfall zone, it is generally believed that the monsoon current does not reach this region. However, our results show the presence of induced monsoonal rainfall with rising trend over valley region of Ladakh

and Nubra. Houze *et al.* (2007) and Medina *et al.* (2010) have examined the rainfall over north-west Himalaya and reported that the region is prone to deep convection during the period of monsoon. Later on, Ray *et al.* (2001) also reported that the interaction of the monsoon trough with western disturbances may occasionally cause dense clouding and heavy precipitation in the months of July and August, which might be the reason for unusual heavy rainfall in 2015. Bhan *et al.* (2015) analysed the Leh cloud burst event in 2010 and discussed the increasing impact of south-west monsoon in this region. More importantly, these studies also highlighted the orography factor in creating heavy rainfall events over a small and compact region surrounded by mountains. Thus, increased precipitation amount in this region has led to hazard vulnerability, mainly in terms of transportation of debris along with the rain water running downstream. This has been further discussed in succeeding sections.

5.2 *Debris flow susceptible zones*

A weighted overlay hazard rating methodology was employed integrating remote sensing, GIS and NWP technique. All raster datasets of terrain parameters such as slope, aspect, curvature, etc., were resampled using bilinear interpolation technique. Nearest neighbour technique was employed for categorical data such as soil and land cover raster before WOA. As dynamic rainfall intensity was considered as a triggering parameter for various debris flow events in the region, the model was run in following two phases:

5.2.1 *Phase 1: Susceptible zones identified based on mean summer precipitation*

In first phase, mean summer precipitation for the period 1997–2017 was provided in the model along with other causative factors. The susceptible map of study area is classified into four hazard risk categories: very low risk, low risk, medium risk and high risk. The road connectivity to various places and glaciers moves through vulnerable slopes where various debris movements takes place during summer rainfall, thus a risk map is prepared for non-glaciated terrain as shown in figure 6. Figure 6 depicts hotspots of the high debris flow susceptible zones from Leh to Siachen glacier and Leh to Turtuk (via Diskit). The high risk zones accounted for 9.45% of land areas in the susceptibility map,

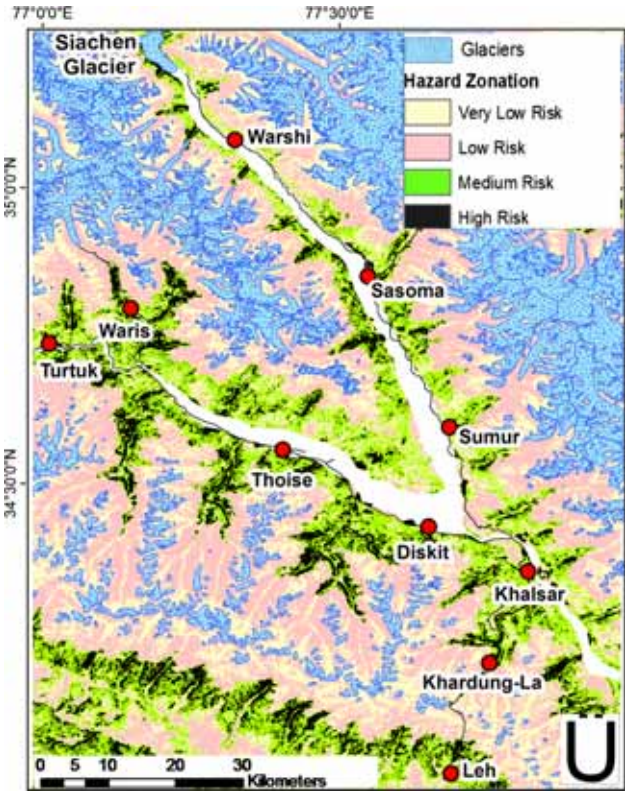

Figure 6. Map showing debris flow susceptible zones derived using weighted overlay technique.

Table 4. *Statistics of debris flow susceptibility zones based on Phase-1.*

Class	Area (km^2)	Area coverage (%)
Very Low	2845	41.22
Low	2087	30.18
Medium	1322	19.14
High	653	9.45

while about 19.14% is classified under medium risk hazard zone (table 4). Most of the slope failures over high vulnerability zones take place on the road and blockage to roadside drains and carriageway. With total road length of ∼92 km from Diskit to Turtuk and ∼106 km from Diskit to Siachen glacier, the affected road length in hazard map is found to be ∼45 km and ∼37 km respectively, and thus more number of high risk zones is found along Diskit and Turtuk.

The susceptible zones identified by Phase 1 are overall hotspots in the region. Their class of vulnerability may change depending upon the main causative factor, i.e., rainfall being dynamic in nature. For this, two different cases of heavy

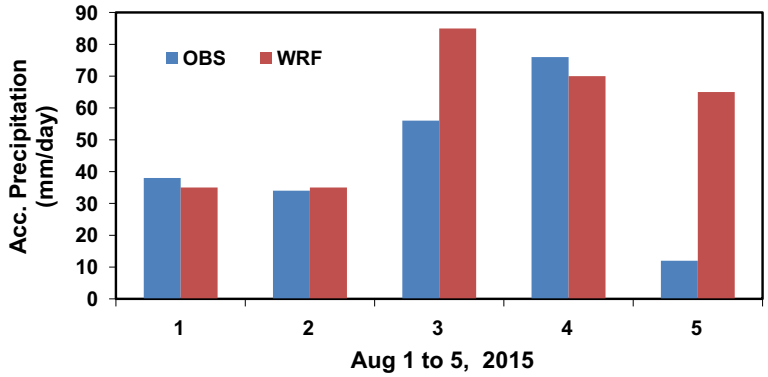

Figure 7. Comparison of WRF 5-day precipitation forecast and gauge-based rainfall observations.

rainfall events simulated by WRF were incorporated into GIS model as discussed in the next section.

5.2.2 *Phase 2: Based on WRF simulation for heavy rainfall events*

Second phase involves prototype for early prediction of debris flow zones based on two heavy rainfall events simulated using WRF model. One of the critical points for proper early prediction of rainfall induced debris flow events is an accurate prediction of temporal intensity of rainfall, for which we compared WRF simulated precipitation with rain gauge observations. The comparison is carried out for one of the heavy rainfall events in 2015 at Thoise. The model simulated 4-days precipitation is found to be in good agreement with gauge observation (r = 0.76) having RMSE and MAE of 13.23 and 8.75 mm/day respectively (figure 7). However, the complete 5-day accumulated precipitation forecasts is found relatively in lesser agreement (r = 0.50) compared to 4-day accumulated forecasts. This may be due to insufficient parameterizations of NWP beyond 3–4 days forecasts over high mountainous regions (Norris *et al.* 2017). The WRF simulated quantitative precipitation was further incorporated into the GIS model to map probable hazard zones during heavy precipitation events.

Figure 8(a) shows spatial distribution of 5-day accumulated precipitation by WRF as well as susceptibility map of debris flow zones during the period 1–5 August 2015. During this event, a mesoscale convective system (MCS) was developed over the Tibetian Plateau (TP) along with the rain storm fronts arriving towards the Nubra valley. In the meantime, a westerly upper air advection also contributed in sustaining this system which led to heavy rainfall events in the region during 1–5 August, 2015 (Ziegler *et al.* 2016). It was also observed from field data that during 19–23 July 2015, a small duration of precipitation maintained high soil moisture in this region (figure 9). The WRF simulated precipitation showed more than 200 mm in 5 days during event period at multiple pockets of study region and thus induced several debris flow events.

Figure 8(b) represents the scenario during Leh cloud burst event period (1–5 August, 2010) along with the susceptibility map. This event was somehow different from above mentioned 2015 event as a diurnal heating of TP region triggered convective initiation of environment of this event towards the Leh region (Rasmussen and Houze 2012). Conversely, a monsoon trough also interacted with MCS which formed intense convective group of clouds over Leh region (Kumar *et al.* 2012; Thayyen *et al.* 2013). Our results showed that over the Leh region the WRF simulated precipitation for 5-Day has accumulated above 200 mm, which led high risk prone zones to Leh region.

From figure 8(a–b), it can be observed that different hotspots of debris flow were identified during these events. While regions from Khalsar to Sumur, Sumur to Sasoma, and Thoise to Turtuk were identified as high risk zones during 2015 event, these were found medium to low risk zones during 2010 cloud burst event. Similarly during 2010 event, apart from Leh, Khardung-La pass and regions of sloped terrains near Diskit was found highly susceptible to debris flow events. The overall comparison of identified hotspots in both the above discussed cases is shown in table 5. It was found in good spatial agreement with field observations.

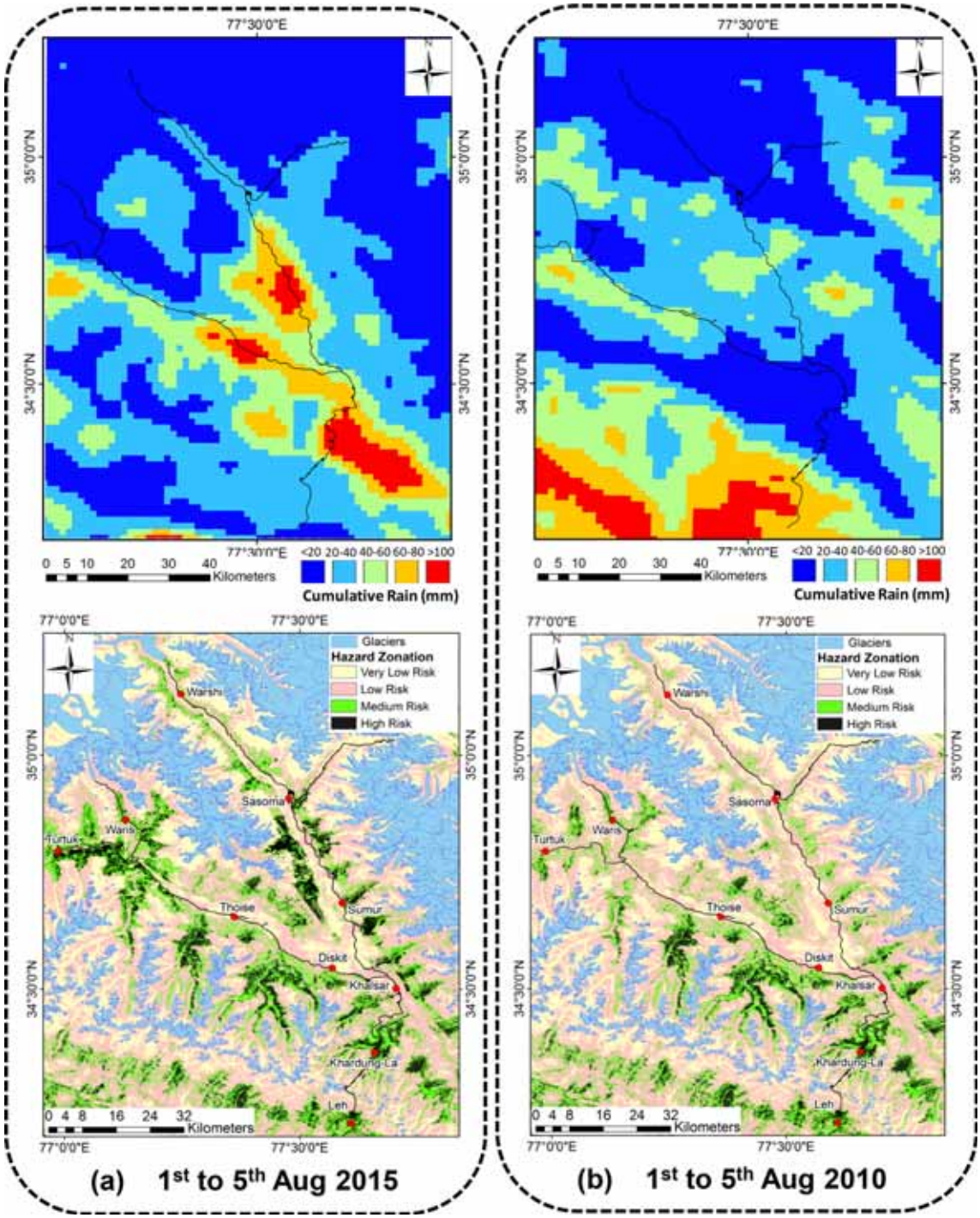

Figure 8. Two cases studies of debris flow events: (**a**) WRF simulation for period 1st to 5th August 2015 and corresponding susceptibility debris flow zonation; (**b**) WRF simulation for period 1–5th August 2010 and corresponding susceptibility debris flow zonation.

5.3 *Model validation*

Field survey was conducted in the September month in Nubra after the debris flow events of 2015. Field identified hazard locations were collected using GPS. Later these hazard locations were overlaid on modelled susceptible classes, i.e., very low risk, low risk, medium risk and high risk and the comparison was made. Besides, Landsat image of period 10th May and 14th October, 2015 was also analysed. For better detection of pre and post changes, image pan sharpening technique was employed using OLI multispectral (30 m) and panchromatic band (15 m), and debris flow zones were identified. It was observed that most of the identified field events occurred over the sloped

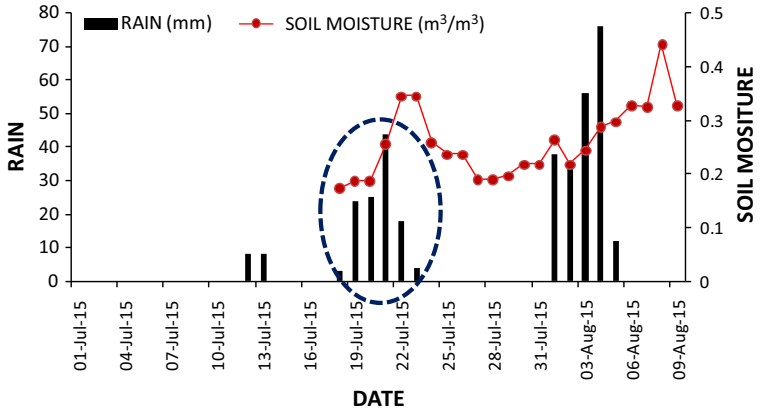

Figure 9. Observational data from Thoise station for July-Aug period. Short duration of rain was observed between 19th July and 23rd July 2015 which maintained high soil moisture (source: SMAP L-Band radiometer data; https://www.mosdac.gov.in/soil-moisture-0) in the region.

Table 5. *An overall comparison of identified hotspots in two cases studied.*

Class	Area (km^2)	Area coverage (%)	High risk zones
Case I (2015 event)			
Very Low	2839.22	41.13	Khalsar–Sumur, Sumur–Sasoma, Thoise–Turtuk
Low	2407.78	34.88	
Medium	1212.17	17.56	
High	443.86	6.43	
Case II (2010 event)			
Very Low	3152.61	45.67	Leh, Khardung-La, Nearby Diskit region
Low	2790.89	40.43	
Medium	728.96	10.56	
High	301.66	4.37	

terrains alongside the road which subsequently hampered the connectivity over Ladakh–Nubra region. For instance, we can see from figure 10 that the debris (mostly boulders and alluvial fanned materials) sliding have occurred near Diskit town and regions between Sasoma and Siachen glacier after heavy rainfall events of 2015. These are mainly the habitat areas. The observed debris flow locations were compared with WRF based hazard risk zones for the 2015 event (figure 10a). Landsat-8 imageries were also utilized to infer changes caused due to debris flow at Thoise. The post event image clearly showed changes like disconnection of roads and flow of debris materials.

After visual based validation, the model performance was checked for 2015 events using statistical predictive Receiver Operating Characteristics (ROC) curve. ROC is widely popular technique for evaluating the accuracy and effectiveness of the susceptibility model (Lee 2005). ROC curve shows model performance based on the true positive rate (TPR) and false positive rate (FPR) (Pradhan 2010). An important measure of the accuracy of the analysis under this predictive curve is the area under curve (AUC). The most ideal model will have the largest area under the curve. An AUC value close to 1.0 presents an ideal model whereas AUC value close to 0.5 indicates inaccuracy of the model. The ROC was thus produced by plotting landslide occurrences (TPR) at y-axis and landslide susceptibility index (FPR). With limited field identified landslide evidences, the collected points were compared with 4 classes of susceptibility map and the curve generated provides rate of success in the model. The computed area under the curve is 0.76, which showed an accuracy of 76.6% for the final susceptibility map (figure 10b).

5.4 *Critical rainfall thresholds*

An analysis on the critical threshold value to induce debris flows was carried out for the study region using ground rainfall observations and WRF estimates. This was evaluated over Thoise for 2015

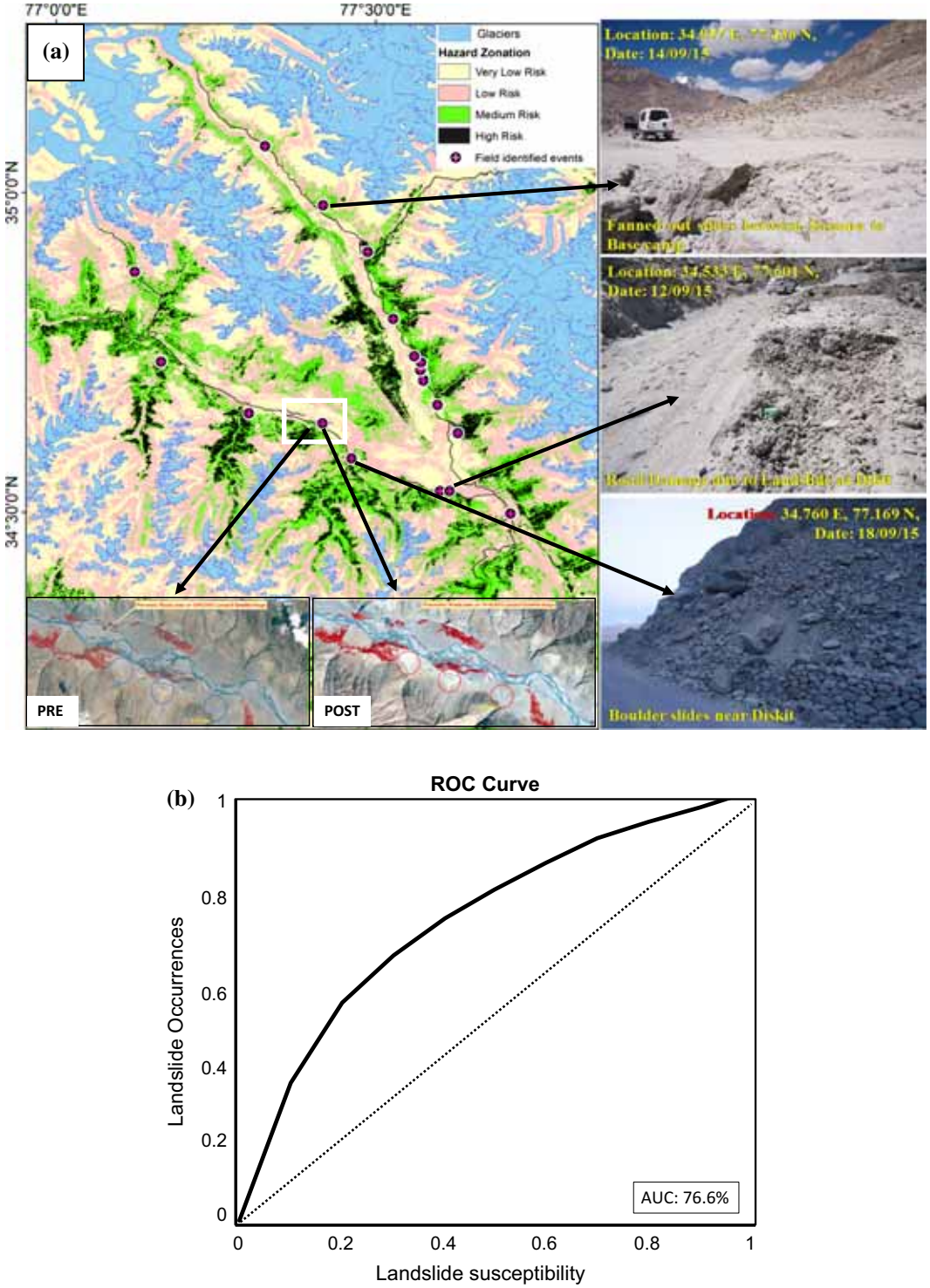

Figure 10. (**a**) Validation of retrieved susceptibility zones of 2015 debris flow events in Nubra valley using field survey and satellite data and (**b**) Assessment of susceptibility map performance for 2015 events based on ROC (normalized over both the axes).

event. Cumulative precipitation (mm/day) was calculated from WRF and ground station till the event occurrence day, i.e., 4th August 2015 (figure 11). The cumulative precipitation for 4 days based on ground observation was 204 mm, which on daily basis estimated threshold value as 51 mm. The model simulation was able to capture the quantitative accumulated precipitation (225 mm) in 4 days and thus was found in agreement with the ground observation. Kirschbaum *et al.* (2012) studied and tested various rainfall triggered debris flow events based on TRMM estimates over the Himalayan arc

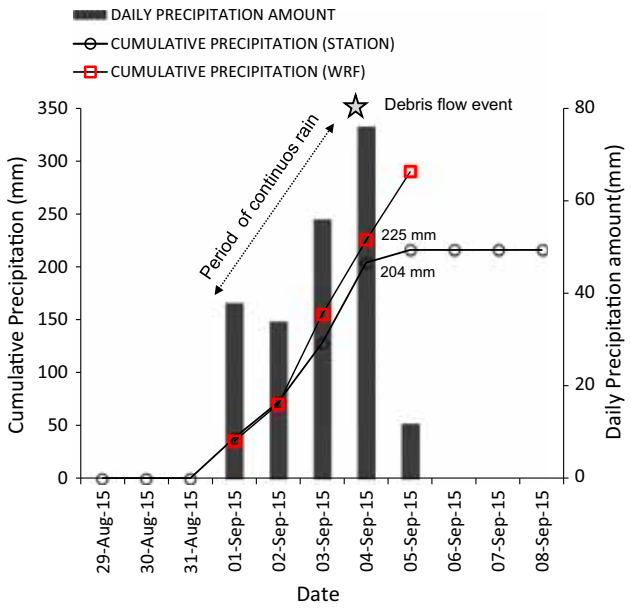

Figure 11. Daily and cumulative rainfall from gauge station and WRF during heavy rainfall period at Thoise.

and reported a threshold amount of 79 mm/day for potential triggering. This showed the threshold value for Nubra region is less compared to other region of Himalaya, which is evident as the Nubra region has glacier deposits, loose landforms and devoid of vegetation.

6. Conclusions

The intense and prolonged rainfall induced debris flow events can cause serious damages to people and social economic progress. To avoid this in Ladakh–Nubra region, there is a need of better understanding of the increased vulnerability from debris flows which gets trigger during prolonged heavy rainfall; such events were in years 2010 and 2015. Analysis based on field information of rainfall intensity for summer-monsoonal period indicated significant rise during the last 20 years, which has caused upsurge in several water induced hazards over this region. The debris flow susceptibility map was produced using WOA method. Seven important causative factors of debris flow occurrence were considered for construction of thematic data layers using GIS. The susceptibility map classified the study area into very low risk, low risk, medium risk and high risk. The map revealed that ∼28% area falls in high and medium risk susceptibility zones. The present study also attempts to identify debris flow susceptible zones in Ladakh–Nubra region by integrating high spatio-temporal WRF information with other causative factors. Two cases of heavy precipitation event occurred in the year 2010 and 2015 were modeled using WRF for assessing debris flow susceptible zones. The investigated area was again divided into four classes of susceptibility which showed that the debris zone has been exposed on alluvial fans of several mountain streams in the area.

The approach used in this study is simple and effective, provides quick results and can be rationalised depending on various factors. This would help in disaster preparedness for the region since this region is facing climate change impacts since last decades. Satellite based estimates based on TRMM have already reported increased heavy rainfall and extreme events over Leh–Ladakh region (Bharti *et al.* 2016). Our study based on field observation supports these on-going changes in rainfall pattern. The reappearance of heavy rainfall causing flash floods and debris flows in the summer-monsoon suggests upsetting situation in this high mountain desert. As per the future climate change scenario the most of the study suggests there will be an increase in precipitation and temperature over the region (Chaturvedi *et al.* 2012). Thus apart from increasing precipitation, increase in temperature over these permafrost regions due to global warming will enhance the probability of larger mass movement events (Huggel 2009). Though the studied region is scanty populated, but because of strategic reason it is generally fully occupied. Due to increasing requirements of locals for different resources such as water, agriculture land, transportation etc., the area mostly remains habitat along the river bed or drainage (alluvial areas). Therefore, there is an urgent need to safeguard the people and infrastructure in this region from increasing extreme events in climate change scenarios. This can be done by either passive method i.e. issuing forecast or by active methods, i.e., control methods. For high risk zones as identified from the present study (table 5), control structure measures, such as, diversion/protection wall or water channel, along the eroded nallahs can be constructed to divert or channelized the water/debris flow. Therefore, the present study may be useful for the decision/policy makers as well as locals to minimise the rainfall induces hazards in the region.

Acknowledgements

The authors are thankful to Director SASE for motivation and support to this work. We thank the

technical persons of SASE Roshan Tamang, G Arun, Ritesh Mujawdiya, and Bhupinder Kumar for field data collection. We are grateful to Air Force Station, Thoise for providing the meteorological data. We would like to acknowledge various institutions for providing gridded CRU precipitation products, ASTER DEM and Landsat-8 data. This work was carried out under DRDO project 'Him-Parivartan'.

References

Adhikari D P and Koshimizu S 2005 Debris flow disaster at Larcha, upper Bhotekoshi Valley, central Nepal; *Island Arc.* **14** 410–423.

Barrett K and Bosak K 2018 The role of place in adapting to climate change: A case study from Ladakh, western Himalayas; *Sustainability* **10** 898.

Basharat M, Shah H R and Hameed N 2016 Landslide susceptibility mapping using GIS and weighted overlay method: A case study from NW Himalayas, Pakistan; *Arab. J. Geosci.* **9** 292.

Bhan S C, Devrani A K and Sinha V 2015 An analysis of monthly rainfall and the meteorological conditions associated with cloudburst over the dry region of Leh (Ladakh), India; *Mausam* **66(1)** 107–122.

Bharti V, Singh C, Ettema J and Turkington T A R 2016 Spatiotemporal characteristics of extreme rainfall events over the Northwest Himalaya using satellite data; *Int. J. Climatol.* **36** 3949–3962.

Bhutiyani M R, Kale V S and Pawar N J 2010 Climate change and the precipitation variations in the north-western Himalaya: 1866–2006; *Int. J. Climatol.* **30(4)** 535–548.

Biswas S S and Pal R 2016 Causes of landslides in Darjeeling Himalayas during June–July, 2015; *J. Geogr. Nat. Disast.* **6** 173.

Blais-Stevens A and Behnia P 2016 Debris flow susceptibility mapping using a qualitative heuristic method and flow-R along the Yukon Alaska Highway Corridor, Canada; *Nat. Hazards Earth Syst. Sci.* **16** 449–462.

Bookhagen B and Burbank D W 2010 Toward a complete Himalayan hydrological budget: Spatiotemporal distribution of snowmelt and rainfall and their impact on river discharge; *J. Geophys. Res.* **115** F03019.

Calligaris C, Poretti G, Tariq S and Melis M T 2013 First steps towards a landslide inventory map of the Central Karakoram National Park; *Eur. J. Remote Sens.* **46** 272–287.

Chaturvedi R K, Joshi J and Jayaraman M 2012 Multi-model climate change projections for India under representative concentration pathways; *Curr. Sci.* **103(7)** 791–802.

Chauhan S, Sharma M, Arora M K and Gupta N K 2010 Landslide susceptibility zonation through ratings derived from artificial neural network; *Int. J. Appl. Earth Obs.* **12** 340–350.

Chevuturi A, Dimri A P, Das S, Kumar A and Niyogi D 2015 Numerical simulation of an intense precipitation event over Rudraprayag in the central Himalayas during 13–14 September 2012; *J. Earth Syst. Sci.* **124(7)** 1545–1561.

Chundawat R S and Rawat G S 1994 In: *Proceedings of the Seventh International Snow Leopard Symposium; International Snow Leopard Trust, Seattle*, pp. 127–132.

Congalton R G, Gu J, Yadav K, Thenkabail P and Ozdogan M 2014 Global land cover mapping: A review and uncertainty analysis; *Remote Sens.* **6** 12,070–12,093.

Crosta G B and Frattini P 2003 Distributed modelling of shallow landslides triggered by intense rainfall; *Nat. Hazards Earth Syst. Sci.* **3** 81–93.

Dou J, Bui D T, Yunus A P, Jia K, Song X, Revhaug I, Xia H and Zhu Z 2015 Optimization of Causative Factors for Landslide Susceptibility Evaluation Using Remote Sensing and GIS Data in Parts of Niigata, Japan; *PLOS ONE* **10(7)** e0133262.

Dwyer J, Roy D, Sauer B, Jenkerson C, Zhang H and Lymburner L 2018 Analysis ready data: Enabling analysis of the Landsat archive; *Remote Sens.* **10(9)** 1363.

Elkadiri R, Sultan M, Youssef A M, Elbayoumi T, Chase R, Bulkhi A B and Al-Katheeri M M 2014 A remote sensing-based approach for debris-flow susceptibility assessment using artificial neural networks and logistic regression modeling; *IEEE J. Sel. Top. Appl. Earth Observ Rem. Sens.* **7(12)** 4818–4835.

Gebremichael M and Hossain F 2010 *Satellite rainfall applications for surface hydrology;* Dordrecht: Springer Netherlands **3** 22.

Gupta P, Khanna A and Majumdar S 2012 Disaster management in flash floods in Leh (Ladakh): A case study; *Indian J. Comm. Med.* **37(3)** 185–190.

Haeberli W, Wegmann M and MUhll D V 1997 Slope stability problems related to glacier shrinkage and permafrost degradation in the Alps; *Eclogae Geol. Helv.* **90** 407–414.

Harris I, Jones P D, Osborn T J and Lister D H 2014 Updated high-resolution grids of monthly climatic observations – the CRU TS3.10 Dataset; *Int. J. Climatol.* **34** 623–642.

Hengl T, Mendes J J, Heuvelink G B M, Ruiperez G M and Kilibarda M *et al.* 2017 Soil Grids 250 m: Global gridded soil information based on machine learning; *PLOS ONE* **12(2)** e0169748.

Hobley D E J, Sinclair H D and Mudd S M 2012 Reconstruction of a major storm event from its geomorphic signature: The Ladakh floods, 6 August 2010; *Geology* **40** 483–486.

Houze R A Jr, Darren C W and Smull B F 2007 Monsoon convection in the Himalayan region as seen by the TRMM Precipitation Radar; *Quart. J. Roy. Meteorol. Soc.* **133** 1389–1411.

Huffman G J, Adler R F, Bolvin D T, Gu G, Nelkin E J and Bowman K P 2007 The TRMM multi-satellite precipitation analysis: Quasi-global, multi-year, combined-sensor precipitation estimates at fine scale; *J. Hydrometeorol.* **8(1)** 38–55.

Huggel C 2009 Recent extreme slope failures in glacial environments: Effects of thermal perturbation; *Quat. Sci. Rev.* **28** 1119–1130.

Juyal N 2010 Cloud-burst triggered debris flows around Leh; *Curr. Sci.* **99(9)** 1166–1167.

Kanwal S, Atif S and Shafiq M 2017 GIS based landslide susceptibility mapping of northern areas of Pakistan, a case study of Shigar and Shyok Basins; *Geomat. Nat. Haz. Risk* **8(2)** 348–366.

Kayastha P, Bijukchhen S M, Dhital M R and De Smedt F 2013 GIS based landslide susceptibility mapping using a fuzzy logic approach: A case study from Ghurmi-Dhad

Khola area, Eastern Nepal; *J. Geol. Soc. India* **82(3)** 249–261.

Khan H, Shafique M, Khan M A, Bacha M A, Shah S U and Calligaris C 2019 Landslide susceptibility assessment using Frequency Ratio, a case study of northern Pakistan; *Egypt. J. Remote Sens. Space Sci.* **22** 11–24.

Kirschbaum D and Stanley T 2018 Satellite-based assessment of rainfall-triggered landslide hazard for situational awareness; *Earth's Future* **6** 505–523.

Kirschbaum D, Adler R, Adler D, Peters-Lidard C and Huffman G 2012 Global Distribution of Extreme Precipitation and High-Impact Landslides in 2010 Relative to Previous Years; *J. Hydrometeor.* **13** 1536–1551.

Kumar M S, Shekhar M S, Rama Krishna S S V S, Bhutiyani M R and Ganju A 2012 Numerical simulation of cloud burst event on August 05, 2010, over Leh using WRF mesoscale model; *Nat. Hazards* **62(3)** 1261–1271.

Lee S 2005 Application of logistic regression model and its validation for landslide susceptibility mapping using GIS and remote sensing data; *Int. J. Remote Sensing* **26(7)** 1477–1491.

Lepore C, Kamal S A, Shanahan P and Bras R L 2011 Rainfall-induced landslide susceptibility zonation of Puerto Rico; *Environ. Earth Sci.* **66(6)** 1667–1681.

Liao Z, Hong Y, Wang J, Fukuoka H, Sassa K, Karnawati D and Fathani F 2010 Prototyping an experimental early warning system for rainfall-induced landslides in Indonesia using satellite remote sensing and geospatial datasets; *Landslides* **7(3)** 317–324.

Long N T and De Smedt F 2019 Analysis and mapping of rainfall-induced landslide susceptibility in a Luoi district, Thua Thien Hue province, Vietnam; *Water* **11(1)** 51.

Lu N, Sener-Kaya B, Wayllace A and Godt J W 2012 Analysis of rainfall induced slope instability using a field of local factor of safety; *Water Resour. Res.* **48(9)** W09524.

Martha T R, Roy P, Govindharaj K B, Kumar V K, Diwakar P G and Dadhwal V K 2015 Landslides triggered by the June 2013 extreme rainfall event in parts of Uttarakhand state, India; *Landslides* **12** 135–136.

Mathew J, Babu D G, Kundu S, Kumar V K and Pant C C 2014 Integrating intensity-duration-based rainfall threshold and antecedent rainfall-based probability estimate towards generating early warning for rainfall-induced landslides in parts of the Garhwal Himalaya, India; *Landslides* **11(4)** 575–588.

Medina S, Houze R A Jr, Kumar A and Niyogi D 2010 Summer monsoon convection in the Himalayan region: Terrain and land cover effects; *Quart. J. Roy. Meteor. Soc.* **136** 593–616.

Miller D J and Burnett K M 2008 A probabilistic model of debris-flow delivery to stream channels, demonstrated for the Coast Range of Oregon, USA; *Geomorphology* **94** 184–205.

Mourre L, Condom T, Junquas C, Lebel T, Sicart J E, Figueroa R and Cochachin A 2016 Spatio-temporal assessment of WRF, TRMM and in situ precipitation data in a tropical mountain environment (Cordillera Blanca, - Peru); *Hydrol. Earth Syst. Sci.* **20** 125–141.

Negi S S 1995 *Cold deserts of India*; Indus Publishing Company, New Delhi.

Negi H S and Kanda N 2019 An appraisal of spatio-temporal characteristics of temperature and precipitation using gridded datasets over NW Himalaya; Climate Change and the White World; Springer (in press).

Nikolopoulos E I, Crema S, Marchi L, Marra F, Guzzetti F and Borga M 2014 Impact of uncertainty in rainfall estimation on the identification of rainfall thresholds for debris flow occurrence; *Geomorphology* **221** 286–297.

Norris J, Carvalho LMV and Co-authors 2017 The spatiotemporal variability of precipitation over the Himalaya: Evaluation of one-year WRF model simulation; *Clim. Dyn.* **49** 2179.

Ochoa A, Pineda L, Crespo P and Willems P 2014 Evaluation of TRMM 3B42 precipitation estimates and WRF retrospective precipitation simulation over the Pacific–Andean region of Ecuador and Peru; *Hydrol. Earth Syst. Sci.* **18** 3179–3193.

Owen L A, Kamp U, Khattak G A, Harp E, Keefer D K and Bauer M 2008 Landslides triggered by the 8 October 2005 Kashmir earthquake; *Geomorphology* **94(1–2)** 1–9.

Pardeshi S D, Autade S E and Pardeshi S S 2013 Landslide hazard assessment: Recent trends and techniques; *SpringerPlus* **2** 523.

Pradhan B 2010 Application of an advanced fuzzy logic model for landslide susceptibility analysis; *Int. J. Comput. Int. Syst.* **3(3)** 370–381.

Pradhan S B 2019 July 16 Nepal floods Death toll touches 78 over 17 500 displaced; *The Wire,* https://www.theweek.in/wire-updates/international/2019/07/16/fgn24-nepal-floods-toll.html.

Raj A 2013 Is Ladakh a 'cold desert'? *Curr. Sci.* **104(6)** 687–688.

Rasmussen K L and Houze R A Jr 2012 A flash-flooding storm at the steep edge of high terrain: Disaster in the Himalayas; *Bull. Am. Meteorol. Soc.* **93** 1713–1724.

Ray T K, Sinha D and Guhathakurta P 2001 Landslides in India; India Meteorological Department Pune, pre-published scientific report No. 1/2001 20.

Riad PH, Billib M, Hassan A A, Salam M A and El Din MN 2011 Application of the overlay weighted model and Boolean logic to determine the best locations for artificial recharge of groundwater; *J. Urban Environ. Eng.* **5(2)** 57–66.

Riaz M T, Basharat M, Hameed, N, Shafique M and Luo J 2018 A data-driven approach to landslide-susceptibility mapping in mountainous terrain: Case study from the northwest Himalayas, Pakistan; *Nat. Hazards Rev.* **19** 05018007.

Saaty TL 1980 *The Analytical Hierarchy Process: Planning, Priority Setting, Resource Allocation;* 1st edn, McGraw-Hill New York, ISBN: 0070543712.

Saaty T L 1990 An exposition of the AHP in reply to the paper "remarks on the analytic hierarchy process; *Manag. Sci.* **36(3)** 259–268.

Shit P K, Bhunia G S and Maiti R 2016 Potential landslide susceptibility mapping using weighted overlay model (WOM); *Model. Earth Syst. Environ.* **2** 21.

Skamarock W C and Co-authors 2008 A description of the Advanced Research WRF version 3; NCAR Tech. Note NCAR/TN-475 + STR **113**.

Tewari M, Chen F, Wang W, Dudhia J, LeMone M A, Mitchell K, Ek M, Gayno G, Wegiel J and Cuenca R H 2004 Implementation and verification of the unified NOAH land surface model in the WRF model (Formerly Paper Number 17.5), In: *20th Conference on Weather Analysis and Forecasting/16th Conference on Numerical Weather Prediction*; Am. Meteor. Soc., pp. 11–15.

Thayyen R J, Dimri A P, Kumar P and Agnihotri G 2013 Study of cloudburst and flash floods around Leh, India during August 4–6, 2010; *Nat. Hazards* **65** 2175–2204.

Ventra D and Clarke L E (eds) 2018 Geology and Geomorphology of Alluvial and Fluvial Fans: Terrestrial and Planetary Perspective; Geological Society, London 440.

Vijith H, Krishnakumar K N, Pradeep G S, Ninu Krishnan M V and Madhu G 2013 Shallow landslide initiation susceptibility mapping by GIS-based weights-of-evidence analysis of multi-class spatial data-sets: A case study from the natural sloping terrain of Western Ghats, India; *Georisk: Ass. Manag. Risk Eng. Syst. Geohazards* **8** 48–62.

Wang Y Q, Ma C B and Wang Z F 2019 Prediction of Landslide Position of Loose Rock Mass at Mountain Tunnel Exit; *Adv. Civ. Eng.* **2019** 3535606.

Ziegler A D, Cantarero S I, Wasson R J, Srivastava P, Spalzin S, Chow W T L and Gillen J 2016 A clear and present danger: Ladakh's increasing vulnerability to flash floods and debris flows; *Hydrol. Process.* **30** 4214–4223.

Corresponding editor: Navin Juyal